EMC2

AD-A257 944

Phenomenological Modelling of Polywell^{tm}/SCIF Multi–Cusp Inertial–Electrostatic Confinement Systems†

Robert W. Bussard and Katherine E. King

EMC2–1191–02

† This work performed under Contract No. MDA–972–90–C–0006 for the Defense Advanced Research Projects Agency, Defense Sciences Office.

EMC2® ENERGY/MATTER CONVERSION CORPORATION
9100 A Center Street, Manassas, VA 22110, (703) 330-7990

PHENOMENOLOGICAL MODELLING OF POLYWELL^{tm}/SCIF MULTI–CUSP INERTIAL–ELECTROSTATIC CONFINEMENT SYSTEMS

I. INTRODUCTION AND BACKGROUND

In an earlier paper[1] (hereinafter referred to as "[I]"), a comprehensive study was made of the recirculation and losses of electrons in their flow through simple inverse power–law potential wells bounded by similarly inverse power–law dependent magnetic fields. This study examined electron flow and loss behavior in the simplest approximation invoked to describe Polywell^{tm} confinement systems. The importance of this study, and of the present paper, is that the power balance in Polywell^{tm} systems is determined entirely by the rate of electron losses; if these are large, then the system can not yield net power.

As noted in [I], a large body of work has been undertaken over the past 35 or so years in the study of general cusp confinement of plasmas[2, 3, 4, 5]. Nearly all of this has examined single particle electron (or ion) motion or the motion of particles in neutral plasmas within cusped magnetic systems, generally without internal electric potential fields. Furthermore, almost all of this work on plasmas has been limited to plasmas in local thermodynamic equilibrium (LTE); none applied to non–neutral systems. Nearly all were without internal E fields; all particles studied were at constant (fixed) total kinetic energy throughout the system. And, almost all of the prior work focussed on spindle–shaped biconic cusps[6] – which are uniquely unable to satisfy the configuration criteria necessary for effective electron confinement in Polywell^{tm}–type multicusp systems.

These special polyhedral configurations[7, 8] allow formation of stable deep electrostatic potential wells in electron/ion mixtures by radial injection of energetic electrons into plasmas with net negative charge. Their spatial characteristics combined

with the distribution of the internal E field arising from electron injection, and the induced predominantly–radial ion motion, can result in long confinement times (due to many recirculation passes through the well before escape) for the electrons[9]. This is the *sine qua non* for minimum electron energy losses, under the conditions of large ion energy and core density achieved by the trapping of ion motion by the electron–driven internal potential.

In this note the problem of electron motion, confinement and losses is analyzed in the non–LTE, electron–rich plasma system with anisotropic radial energy in both species, in multicusp Polywell^{tm} geometry. The bulk problem is treated as one–dimensional, with arbitrary spatial indices of radial B and E field variation. Here, unlike [I], the B field is taken to have a "rollover" shape, consistent with the results of computer calculations of actual field distributions in polyhedral systems, that follows a simple power–law within the system but departs from it as the system boundary is approached from within.

An important feature of the Polywell^{tm} system is the possibility of inducing B field distortion by bulk diamagnetic collective effects arising from diamagnetic currents induced in the motion of electrons by their interaction with the basic field geometry. These diamagnetic currents will act to exclude the B field from the interior of the system; an effect which will lead to a B field shell, compressed to a $\beta = 1$ condition, surrounding and confining the central electron cloud in the system. These effects are crudely modelled as they influence this 1–D spatial variation of B field, but electron entry into single cusp volumes includes elements of the geometric effects of the real 3–D configuration. Electron motions in mirror reflection regions are analyzed on the usual basis of conservation of magnetic moment of the electron at entry into the confining cusp. However, turning points of this motion are modified to account for the effects of diamagnetic currents on this process.

In the discussion here, it is helpful to define several terms for critical radii within the system. The electrons are modelled as originating at the system center, at r = 0, moving through a non–adiabatic region to that radius (r_b) at which the electron "$\beta = 1$", thence to that radius (r_{ad}) at which adiabatic reflection will occur in the cusp fields, and finally to the outer radius, r = R, of the system.

II. MIRROR/WIFFLE–BALL MODE OPERATION

There are two distinct modes of operation in the system. The first operating scheme is to establish the system with maximum B field, and turn on a small electron current at maximum (desired) electron energy, followed by injection of ions controlled so as to yield the desired central virtual anode height in the system. It has been shown by Bussard and King[10] that this control must be relatively precise (e.g. within a factor of 2–4x) in order to avoid "blowout" of the well by excessive ion density. Given a controllable ion source, and similarly controllable electron injection, the system can be driven to higher core density by injection of ever–increasing electron current with corresponding ion input.

This mode of operation ensures that the system will start as a mirror confinement system for, at low electron density, $\langle r_b \rangle = (r_b/R)$ is very small compared to $\langle r_{ad} \rangle = (r_{ad}/R)$ and the only physics initially able to retain the electrons is that of reflection in the cusp fields; no diamagnetic $\beta = 1$ fields have yet been established. Once started in this mirror reflection (MR) mode, continued increase in electron injection current drives the $\beta = 1$ radius, $\langle r_b \rangle$, to larger values so that some internal reflection within the diamagnetic sphere adds to the confinement due to continuing MR effects. It is important to note that the electron recirculation due to the MR contribution is severely

limited by the considerable depth of the negative potential well created by the (desired) excess electron charge in the system.

In contrast with electron motion under conservation of magnetic moment in field–free cusp systems, the confining effect of the magnetic moment conservation process is greatly reduced here by the presence of the internal E field. This acts to accelerate the electrons outwards in the system, and adds radial energy to their motion almost as fast as the cusp–trapped transverse energy increases and takes it from radial motion. In fact, if the well depth were to become exactly equal to the electron injection energy (a physical impossibility so long as ions are present), the cusp fields would not confine the electrons at all. The MR mode works, but only poorly if the system has a deep potential well.

The general model of electron motion in the system for this mode of startup and operation was discussed and illustrated further in [I], which showed the linear approximation used for variation of the adiabaticity radius, $<r_{ad}>$, in modelling the transition from the MR mode to the diamagnetic $\beta = 1$ mode. Examining this mode in some more detail, once the electrons have reached a radial distance (r_x) at which their local gyro–magnetic radius is sufficiently small that the total area of all of their gyro radius circles from each of the cusps is equal to the area of the spherical surface at that radius, they will enter one or another cusp in their outward motion. If r_b is less than this "transition radius" r_x the electrons move non–adiabatically without confinement, and enter the spatial domain of each cusp at r_x. No diamagnetic effects are yet functional at this point, as the gyro radius of electrons within $r_b < r_x$ is greater than the gyro radius at r_x, and coherent currents counter to the external B fields can not be generated and sustained.

Once r_b becomes greater than r_x the electrons inside r_b will "see" a lossy sphere with surface loss area (due to gyro radius area "holes") that is smaller than the sphere area

at r_b, and they will be confined by internal reflection within this diamagnetic $\beta = 1$ sphere. The average number of transits an electron will make within this sphere at r_b is just the ratio of the sphere area to the total loss area. As r_b grows larger (with increasing electron current input, and increasing central density – with requisite additional ions to maintain charge balance) this confinement grows larger, because the fractional hole loss area becomes smaller due to increasing B field strength at larger radial positions. This can be thought of as the confinement of a particle inside a perfectly–reflecting spherical shell perforated by holes – like the "wiffle ball" toy; and it is called "wiffle–ball" (WB) confinement. The average number of transits within r_b is defined here as G_{jwb}.

At some radius (r_{ad}) set by the mirror adiabaticity requirement that the local B field change only little over a local gyro radius, the electron is trapped in "mirror–reflection" (MR) oscillation within the cusp. Electron trapping in this (MR) mode is by the usual form of mirror reflection coefficient for motion in a single cusp mirror system[1*]. This can be used to find a measure of the average number of transits G_{jmr} that an electron will make between $r_{ad} < r < R$ within this cusp mirror geometry.

[1*] The form for mirror reflection coefficient involves a term which is the square of the sine of the minimum trapping angle (relative to the B field) of electron motion in the B field at r_{ad}, the trapping radius, for their escape at radius r=R. In the case of a system with electrons at constant energy and a B field varying as $\langle r \rangle^m$ this term varies as $\langle r_{ad} \rangle^m$. In the present case, the simultaneous radial variation of the E field reduces the reflection coefficient by virtue of the acceleration of electrons out of the system by the potential well gradient. If this E field is equal in magnitude to, and varies with the same functional form as the B field, no mirror trapping will be possible in the system. If the potential well is less deep than the electron injection energy, trapping is still possible, but with the reflection coefficient term reduced by a factor of about $(1 - \alpha_q)$, where $\alpha_q = e\Phi_o/E_o$ is the ratio of well depth to injection energy.

As r_b grows beyond r_x it begins to distort the externally–imposed polyhedral B field distribution to yield a configuration in which the field is compressed outwards by continuing expansion of the "$\beta = 1$" surface (r_b). This results in the displacement of the adiabaticity radius (r_{ad}) to larger radii at a rate such that, with full diamagnetic currents, it will always fall outside the "$\beta = 1$" radius. Thus r_{ad} recedes outwards as r_b exceeds r_x.

Eventually r_b and r_{ad} reach a critical radius r_k at which further radial growth of r_b becomes unstable with respect to r. This is because the magnetic pressure balance criterion is satisfied for all radii beyond r_k, once it is reached at r_k. This radial position is that at which the electron (and ion) density begins to increase rapidly with $r > r_k$. Up to $r < r_k$ both ion and electron density fall approximately as $1/r^2$ from the core region at radius r_c with density n_c. Beyond r_k both ion and electron density increase rapidly, and the electron energy increases while the ion energy decreases as $r \rightarrow R$. Beyond r_k the electron density diverges markedly from the ion density in order to satisfy Poisson's equation and produce the desired negative potential well. In a general analysis of particle density distributions, Krall[11] showed that the position of $\langle r_k \rangle$ depends on the the potential well shape. For typical well shapes of interest, $\langle r_k \rangle \approx 0.83$.

Once $r_b = r_k$ on this model, the behavior of the system "jumps" from r_k to R, where all further increase in system density buildup (by increasing electron and ion injection currents) is stopped at the levels relating drive current (I_e) and core density (n_c) attained at the $r_b = R$ condition. This is (obviously) because r_b can not physically become greater than R, even though mathematically this is possible, because the B field falls past $r > R$ and the electron loss area thus increases with increasing r.

In short, the B field can not confine electrons at a density above that at which the surface electron energy density exceeds the energy density of the magnetic field system. Operation at this final condition is pure WB mode, and is at the point where $<r_b> = 1$; all mirror effects have vanished and the electron confinement is due entirely to recirculation within the diamagnetic sphere perforated by loss holes on the cusp axes whose radii are proportional to the on–axis strength of the cusp B fields.

This final $<r_b> = 1$ WB mode operating condition can be reached by an alternate route. The other extreme of startup and operation is to avoid the MR mode entirely, and drive the system from the beginning as a high β diamagnetic device. This can be done, in principle, by starting with any desired electron injection energy but with a greatly reduced B field, so that the $\beta = 1$ surface initially is very far out in the system, $<r_b> \approx 1$. At this condition there will be no mirror reflection, because there is no mirror field region; all of the field is diamagnetically compressed to the outer boundary region, and all electron losses are governed by the WB gyro hole loss mechanisms.[12]

However, with small B fields and large electron energy (as required for the production of wells deep enough to yield ions with high fusion cross–sections) the electron recirculation factor (G_{jo}) will be very much too small to achieve low electron losses and good power balance. In order to reach high G_{jo} values the confining B field, that sets the size of the electron gyro loss holes in the WB sphere, must be increased to a much larger value.

If this is done rapidly, with no increase in electron current, the $\beta = 1$ sphere will be compressed to a radius smaller than $r_b \approx R$, and the WB confinement will be reduced by the increase in gyro hole loss area due to the decreased gross B field at smaller radius, as well as by the smaller size of the confining sphere. If this decrease is sufficiently large, the

system will reach an unstable mode such that the WB sphere will continue to shrink until it stabilizes with the rise of MR mode confinement as r_b falls below r_k. Now, the system has "jumped" to operation in the MR mode, as described above.

However, if the B field is increased slowly (relative to electron lifetime in the system), and in small steps, the system will remain stable along the $<r_b> = 1$ line and can be driven to higher and higher recirculation simply by increasing the B field, without increasing the electron drive current. This method avoids the limiting behavior of the MR mode, and allows attainment of the final state of maximum G_{jo} on the $<r_b> = 1$ line with much less drive current than is required to make the transition from MR to WB mode in the other startup scenario.

In either case, at this final stable state, when $r_b = R$ the core and bulk densities of electrons (and also of ions) are at their maximum values for the parameters defining the system (e.g. I_e, n_c, E_o, B_o, R). Further increase in electron drive current can not increase system density. Since fusion power output is proportional to the square of the core density, and since this is proportional to the surface density – and hence to the square of the B field – it is clear that increasing B field strength has a strong effect on system fusion power generation. On this simple argument, on the $<r_b> = 1$ line, the fusion power will vary as the fourth power of the B field,[13] just as for conventional magnetic confinement machines.

III. ANALYTIC MODELS OF ELECTRON MOTION

In [I] the electron motion was based on a simple monotonic potential well with magnetic field and electron kinetic energy variation according to

$$B(r) = B_o<r>^m \text{ and } E(r) = E_o<r>^m \qquad (1)$$

where $\langle r \rangle = (r/R)$. However, studies[14, 15, 16] have shown that the field variation asymptotically approaches the simple power law form only as the radius becomes smaller (approaching the origin) within the system. At radii beyond about $\langle r \rangle = 0.5$, the field modulus exhibits a "bumpiness", and its variation in any plane section through the center of the system and one of the edge midpoints always shows a "rollover" as the edge of the system is approached.

The effect of this realistic departure from the power law assumed in [I] is beneficial to electron confinement because it gives larger B fields at deeper radii than does the simple power law (for the same face cusp central field strength). The simple model is thus likely to yield results that are conservative (or pessimistic), because of its underestimate of the strength and effects of the real magnetic fields in the system. This can be rectified by employing an improved description of the B field, which better mocks up the actual variation within the polyhedron. Limiting this, as before, to radial–only dependence (1–D can be analyzed in closed form; 2–D can not) it is found that the edge effects can be accounted for in an approximate way by use of

$$B(r) = B_o \langle r \rangle^m f_o(r) = B_o \langle r \rangle^m \left[\frac{2}{(1+\langle r \rangle^{m+2})} \right] \qquad (2)$$

It is obvious from this that the field strength deep within the system will be twice that previously used, for the same value of cusp central–axis maximum field strength, B_o. As a result, the electron gyro radii at these inner radial positions will be roughly one–half of those previously estimated, with concomitant improvement in electron confinement.

This simple formula has the advantage that it will still yield analytic solutions for most (but not all) of the parameters which characterize the system and are used in the solution methods employed in the model of [I] (e.g. the specific dimensionless radii $\langle r_{ad} \rangle$,

$\langle r_b \rangle$, $\langle r_x \rangle$, and the separate mode recirculation ratio terms G_{jmr} and G_{jwb}). Unfortunately, the transit time integrals can not be obtained in useful closed forms with this more realistic potential variation. However, since the transit time segments used in the calculation of the electron recirculation are divided by the total transit time in the expression for the overall system G_{jo} ratio, the effect of integral departures from exact behavior are minimal for this factor, thus these times can be taken from the forms described above (and shown in Figure 1) without serious error.

In the MR startup case, when electron injection is started, the only confining mechanism is mirror–reflection (MR) from the radius r_{ad} to R, over a number of transits G_{jmr}. As electron injection current is increased the WB mode develops when $r_b > r_x$, and the confinement parameter G_{jwb} grows progressively larger than unity. Particles between r_{ad} and r_b simply transit through this space. Since all particles that emerge from r_b (escaping the WB region) enter the MR region at $r < r_{ad}$, the total number of passes that an electron will make before loss is the product of those in each region.

To determine the overall lifetime and mean number of passes made by an electron in the system it is necessary to find these parameters for each mode of confinement, and weight them by the fractional number of electrons participating in each mode. This introduces a weighting factor dependent on $\langle r_b \rangle$. With this and the transit time formulae summarized in Figure (1), it is possible to write[17] the recirculation ratios for the two cases when the system has not yet begun to exhibit WB mode operation (i.e. when $r_b < r_x$) and when the system does show this mode (i.e. $r_b > r_x$). These formulae are given in Figure (2).

Using these formulae it is possible to calculate G_{jo} over a range of the system–defining parameters, (Z) and (W). Note that W is defined by system external

design criteria, while Z is determined by internal conditions reached in the dense core during system operation. It is instructive to examine G_{jo} to see how the MR and WB contributions vary with these parameters.

IV. ANALYSIS: THE GJ CODE

The MR and WB contributions can be calculated separately from their terms in the overall formulae for G_{jo}. Since all of the relevant parametric terms in these equations are given only in implicit form, it was necessary to construct a simple computer code to calculate G_{jmr}, G_{jwb} and G_{jo}. This code, called the GJ code, was used to determine parametric scaling of G_j with Z and W for a wide range of operating and design parameters for the Polywell^{tm} systems of interest. Results of these calculations are shown in a series of figures attached herewith (Figures 3–6). All calculations were made for a truncated cube system with an effective cusp number of $N \approx 8$, a B field spatial index of $m = 3$, a critical density radius of $\langle r_k \rangle = 0.83$, loss radius factors of $k_L = 1, 2, 3$, and for a potential well with virtual anode fractional height of $n = 0.272$.

All the figures show that G_{jmr} drops with increasing Z (increasing core density) beyond the point where $r_b \geq r_x$. This is a result of the decrease in both MR mode time t_{mr} and in the weighting term $(1-\langle r_b \rangle)$, even before $\langle r_b \rangle$ reaches $\langle r_{ado} \rangle$. As $\langle r_b \rangle$ moves beyond $\langle r_{ado} \rangle$ the drop is even faster, as the diamagnetic effects of induced counter–currents in the electron flow become larger and "push" $\langle r_{ad} \rangle$ to larger radii.

Figures (3a–f) and (4) show 2–D plots of the total G_{jo} for $m = 3$ power–law wells with a virtual anode, over a range of Z and W, and for convergence ratio $\langle r_o \rangle = 1E{-}2$ and anode height $\eta = 0.272$. Figures (3a–f) show a wide range of the well depth parameter α_q, from zero (no well) to 0.995. Figure (4) is a plot of just the $\langle r_b \rangle = 1$ line for several

values of the gyro loss radius parameter k_L. As expected, increasing k_L shifts the $<r_b> = 1$ line to higher Z by a factor of k_L^2.

Examination of Figures (3a–f) shows that the well depth affects the MR mode drastically as α_q becomes larger than about 0.8–0.9, and that the character of the parameter phase space changes for larger values than 0.9. In particular, it is found that the MR mode regime bifurcates from the WB mode regime, and develops a characteristic behavior that is antithetical to WB operation. A "valley" appears between these two regimes of operation that subsequent code calculations have shown is very difficult to cross.

Another series of calculations was made to test the effect of anode height on G_{jo}. These showed that the variation of G_{jo} with Z and W is virtually independent of η for all $\eta > 0.01$. At very small $\eta \to 0$ the forms used for the transit time integrals begin to break down and give excessive transit times; for all realistic wells the dependence of G_{jo} on anode height is negligible for $0 < \eta < 0.3$.

It is useful to distinguish three regions of differing character on these figures. In the left hand region below Z ≈ 1E13/cm the electron behavior is completely dominated by mirror–reflection effects. In this area the device is simply a multicusp mirror machine, operating with the usual MR features. In the right hand region above Z ≈ 1E16/cm, electron behavior is completely dominated by collective mode (diamagnetic) wiffle–ball effects, and mirror phenomena in this region have essentially vanished. Here and above (to Z > 1E18/cm) lies the fusion reactor regime. This region is new and unfamiliar to the field of cusp plasma research; it forms the basis for the original Polywell^{tm} concept and the early studies[18] of its characteristics.

In the middle region where 8E13 < Z < 8E15/cm lies all of the physics of transition from MR to WB operation. This region is of experimental and theoretical interest, because of the new and novel physics features found here. However, this transition is significant for operation of these devices in fusion reactor regimes only if the system is started in the MR mode.

A variety of calculations have been made that show the parametric performance across the range from pure WB mode to pure (initial) MR mode. These are summarized for one case in Figure (5) that shows a three–dimensional picture of the two–dimensional portrayal of the earlier figures. From this it is evident that the device can operate either as a mirror machine OR as a wiffle ball machine, but that it can NOT operate as both.

Examination of the calculated data shows that the MR mode (the right hand area of the figures) leads to increased G_j but only at modest Z, not sufficient for power reactor operation. However, starting the system as a WB machine causes it to ride up the $\langle r_b \rangle = 1$ "ridge" line at the left hand side of the figures, always with an increasing G_j. Detailed EKXL code calculations have been made, to test the validity of this GJ code global mapping, that show the drive current required to move up either of these startup paths.

The results show that following the MR mode at small W leads to early increase in G_j, until Z values around those of the $\beta = 1$ line are reached. Beyond this point, to force the machine through the transition from MR to WB modes, in order to get on the $\beta = 1$ line, itself, requires ever–increasing electron drive currents. In contrast, if the device is started with a large W (e.g. by operation at low B field), it can be made to reach the $\beta = 1$ line at small G_j in the WB mode, and then to ride up the $\langle r_b \rangle = 1$ line by slow reduction of W (by slow increase of the B field) to the reactor regime (ca. Z ≈ 1E19/cm) without

significant increase in the current required to reach the $\beta = 1$ line in the first place. This is seen clearly in Figure 7, where the increasing drive currents necessary to transition from MR to WB mode are plotted for a constant W. The final current here is 18 kA, where the current necessary to ride up the $\langle r_b \rangle = 1$ line is less than 1800 A.

Note that the electron recirculation ratio G_{jo} increases more slowly with Z, in the MR mode, once the Z value has passed that for $\beta = 1$ (in the 2–D projections), and that the slope of the G_{jo} vs. Z curve, along a line of constant W first becomes negative, then slowly becomes positive, until it reaches a slope of unity. Below this point the system is grossly stable with respect to increasing drive current input. However, beyond this point the slope exceeds unity, and the system becomes grossly unstable. From this point up to the $\langle r_b \rangle = 1$ line (at which point the device can not be driven further) the current must be reduced, for operation on the $\langle r_b \rangle = 1$ line requires LESS current than to reach the stable regions with slope < 1 below the unstable region under the $\langle r_b \rangle = 1$ line. This can all be avoided by operation along the $\beta = 1$ line, as described above.

Since the value of G_{jo} for MR operation drops with increasing Z, from its initial low–Z value, as operation leaves the MR mode – before WB mode confinement has taken any significant effect – it appears as a "gate" through which machine operation must be driven at startup. This is true only if started in the MR mode and is NOT true if started in the WB mode. If the device is drive–current–limited, and if the current is insufficient (for the design values of minimum W for the machine) to yield Z values (e.g. core densities) beyond this gate region, it will not operate above the much smaller Z value to which the limited current can drive it in the MR mode.

The WB mode does not begin until $r_b > r_x$ and then rises rapidly with increasing Z, t_{wb} and the weighting term $\langle r_b \rangle$. This is quite clearly seen where the G_{jwb} curves fall

rapidly to unity as Z approaches a value of about 1E14/cm from above. The cutoff Z value is determined from the equation for G_{jwb} by setting this equal to unity. Thus, for all values of $Z < N(k_L)^2S^2/2r_e$ the system will be operating solely in the MR mode. This has the inverse consequence that WB mode physics can be tested only if the experimental system is capable of being driven to a core density above this cutoff limit; $n_c(r_c)^2 > N(k_L)^2S^2/16\pi r_e$. Typically, if $r_c = 1$ cm and $N = 8$, then $n_c > 2e11\ 1/cm^3$.

It is very important to note the effects and characteristics anticipated for this device. In particular, a limited–current experiment operating strictly in the MR mode that runs into the "gate" effect will demonstrate poorer electron (and ion) confinement with increasing current and core density. This is to be expected in this regime. Results of such experiments can map out the MR portion of the 3–D parameter space that describes complete system operation, but can not illuminate the physics of operation in the WB regime. This regime is along the $<r_b> = 1$ ridge line in the parameter space of the system, as shown in Figure (5).

This final form of the G_{jo} formalism outlined above (GJ vers. 1.1), has been built into the EKXL code (vers. 4.1), so that this code now incorporates fully correct physics models that describe system behavior across all the possible range of parameter space.[19]

Calculations using this version 4.1 of the EKXL code have been made parametrically for a variety of cases at high density ("reactor") conditions, and for a wide range of models for SCIF experimental systems and operations. Results of the SCIF computations are discussed in a separate EMC2 technical note[20]. Results of the reactor case studies are given in a forthcoming EMC2 technical note. In all of these the effective "loss radius" has been taken to be in the range $2 < k_L < 3$, as derived from elementary considerations[21] of

diamagnetic behavior in the system. Knowledge derived from this work has been used to analyze possibilities for startup of SCIF with neutral background gas; this is reported in another technical note.[22]

LIST OF FIGURES

REFERENCES

[1] Robert W. Bussard and Katherine E. King, "Electron Recirculation in Electrostatic Multicusp Systems: I — Confinement and Losses in Simple Power Law Wells," Energy/Matter Conversion Corp., Technical Report, EMC2–0491–03

[2] I. Spalding, "Cusp Containment," in Advances in Plasma Physics, Vol. x, 1971, pp. 79–123

[3] D.G. Blondin and T.J. Dolan, "Equilibrium plasma conditions in electrostatically plugged cusps and mirrors," Jour. Appl. Phys. Vol. 47, No. 7, July 1976, pp. 2903–2906

[4] P.J. Catto and J.B. Taylor, "Electrostatic Enhancement of Mirror Confinement," Nuclear Fusion, Vol. 24, No. 7, (1984) pp. 229–233

[5] O.A. Lavrent'ev, "Electrostatic and Electromagnetic High–Temperature Plasma Traps," Conference Proceedings, Electrostatic and Electromagnetic Confinement of Plasmas and the Phenomenology of Relativistic Electron Beams, Ann. N.Y. Acad. of Sci., Vol. 251, 1975, pp. 152–178

[6] J. Berkowitz, et al, "Cusped Geometries," Proceedings of the Second International Conference on the Peaceful Uses of Atomic Energy, Geneva, 1958, United Nations, Geneva, Vol. 31, 1958, pp.171–176

[7] R.W. Bussard, "Method and Apparatus For Controlling Charged Particles," U.S. Patent Number 4,826,626, May 2, 1989, assigned to Energy/Matter Conversion Corporation (EMC2)

[8] R.W. Bussard, G.P. Jellison and G.E. McClellan, "Preliminary Research Studies of a New Method for Control of Charged Particle Interactions," Pacific–Sierra Research Corp. Report No. PSR–1899, 30 Nov. 1988, Final Report under Contract No. DNA001–87–C–0052, Defense Nuclear Agency, Sect. 1

[9] R.W. Bussard, "Some Physics Considerations of Magnetic Inertial–Electrostatic Confinement: A New Concept for Spherical Converging–Flow Fusion," Fusion Technology, Vol. 19, No. 2, March 1991, pp. 273–293, Sect. III–C

[10] R.W. Bussard and K.E. King, "Computer Modelling of SCIF Experiment Performance," Energy/Matter Conversion Corp., Technical Report, EMC2–0691–02

[11] N.A. Krall, "Density Profiles in the Polywell^{tm}/SCIF Device," Krall Associates, internal Technical Report, KA–90–51, Dec. 1990

[12] Kaye, A.S., "Plasma Losses Through an Adiabatic Cusp," J. Plasma Physics, Vol. 11, part 1, 1974, pp. 77–91

[13] Bussard, R.W., K.E. King, "Electron Current, Beta Limit Line Operation and Power Balance in WB Mode", Energy/Matter Conversion Corporation Report EMC2–0891–02, August 1991

[14] Op cit ref. 7, Appendix C, p. 189, Figure 2–1, "Magnetic field along square face axis; truncated cube"

[15] N.A. Krall, "The Polywell^{tm}, A Spherically Convergent Ion Focus Concept," Krall Associates, internal Technical Report, KA–90–45, Feb. 1991, to be published in Fusion Technology (1991)

[16] S.K. Wong, "Structure of the Polywell^{tm} Magnetic Fields," Energy/Matter Conversion Corporation, internal Technical Report, EMC2–0391–04, Mar. 1991

[17] Bussard, R.W., K.E. King, "Electron Recirculation in Electrostatic Multicusp Systems: II — System Performance Scaling of One–Dimensional 'Rollover' Wells", Energy/Matter Conversion Corporation

Report EMC2–0791–04, July 1991

[18] Op cit ref. 8, Sect. VI–A

[19] K.E. King, R.W. Bussard, "EKXL: A Dynamic Poisson–Solver for Spherically–Convergent Inertial–Electrostatic Confinement Systems," Energy/Matter Conversion Corp., Technical Report EMC2–1191–03, November 1991 as presented at the American Physical Society Thirty–Third Annual Meeting of the Division of Plasma Physics, Tampa, FL, November 1991

[20] Robert W. Bussard and Katherine E. King, "SCIF Performance from Code Calculations," Energy/Matter Conversion Corp., Technical Report EMC2–0691–02, June/July 1991

[21] Robert W. Bussard, "Effective Gyro Hole Loss Radius and Diamagnetic Limit in Polywell^{tm} Systems," Energy/Matter Conversion Corp., Technical Report, EMC2–0591–02, May, 1991

[22] Robert W. Bussard, "SCIF Startup With Neutral Gas Background," Energy/Matter Conversion Corp., Technical Report, EMC2–0691–03, June/July 1991

Transit Time Calculations for G_{jo}

$$t_{tot} = \frac{2R}{v_{in}} \left[\frac{\langle r_0 \rangle + \left[\frac{\langle r_w \rangle^2 - \langle r_0 \rangle^2}{2\langle r_0 \rangle} \right]}{\left[\eta + \frac{\delta E_w}{2E_0} \right]^{1/2}} + \frac{2}{\left[1 + \frac{\delta E_w}{2E_0} \right]^{1/2}} \left[\frac{1}{\langle r_w \rangle^{1/2}} - 1 \right] \right]$$

For $\langle r_b \rangle < \langle r_w \rangle$:

$$t_{MR} = \frac{2R}{v_{in}} \left[\frac{\left[\frac{\langle r_w \rangle^2 - \langle r_b \rangle^2}{2\langle r_0 \rangle} \right]}{\left[\eta + \frac{\delta E_w}{2E_0} \right]^{1/2}} + \frac{2}{\left[1 + \frac{\delta E_w}{2E_0} \right]^{1/2}} \left[\frac{1}{\langle r_w \rangle^{1/2}} - 1 \right] \right]$$

$$t_{WB} = \frac{2R}{v_{in}} \left[\frac{\langle r_0 \rangle + \left[\frac{\langle r_b \rangle^2 - \langle r_0 \rangle^2}{2\langle r_0 \rangle} \right]}{\left[\eta + \frac{\delta E_w}{2E_0} \right]^{1/2}} \right]$$

For $\langle r_b \rangle > \langle r_w \rangle$:

$$t_{MR} = \frac{2R}{v_{in}} \left[\frac{2}{\left[1 + \frac{\delta E_w}{2E_0} \right]^{1/2}} \left[\frac{1}{\langle r_b \rangle^{1/2}} - 1 \right] \right]$$

$$t_{WB} = \frac{2R}{v_{in}} \left[\frac{\langle r_0 \rangle + \left[\frac{\langle r_w \rangle^2 - \langle r_0 \rangle^2}{2\langle r_0 \rangle} \right]}{\left[\eta + \frac{\delta E_w}{2E_0} \right]^{1/2}} + \frac{2}{\left[1 + \frac{\delta E_w}{2E_0} \right]^{1/2}} \left[\frac{1}{\langle r_w \rangle^{1/2}} - \frac{1}{\langle r_b \rangle^{1/2}} \right] \right]$$

$$\eta_o = \frac{E_{ao}}{E_o} \qquad \eta' = 1 - \alpha_q (1 - \eta_o) \qquad \langle r_w \rangle \approx \langle r_0 \rangle + \left[\frac{2}{m} \langle r_0 \rangle^2 \eta' \right]^{1/(m+2)}$$

$$\frac{\delta E_w}{2E_o} = \frac{1}{2} \left[\langle r_w \rangle^m + \frac{\langle r_0 \rangle^2 \eta'}{\langle r_w \rangle^2} \right] + \frac{1}{2}(1 - \alpha_q) \rightarrow \frac{1}{2}(1 - \alpha_q)$$

Figure 1.

Summary of formulae used for total and partial (segmented) electron transit time calculation in virtual anode wells with "rollover" B field.

Mirror/Wiffle Model for G_{jo}

$$G_{jo} = G_{jMRo}\left[\frac{4}{N}\frac{(1-\langle r_b\rangle)}{(1-\alpha_r)}t_{MR} + \langle r_b\rangle t_{WB}\right]\frac{1}{t_{tot}} \qquad r_b < r_x$$

$$G_{jo} = G_{jMRo}\left[\frac{4}{N}\frac{(1-\langle r_b\rangle)}{(1-\alpha_r)}t_{MR} + G_{jWB}\langle r_b\rangle t_{WB}\right]\frac{1}{t_{tot}} \qquad r_b > r_x$$

where:

$$G_{jMRo} = \frac{1}{\langle r_{ad}\rangle^m}\left[1-\alpha_q(1-\langle r_{ad}\rangle^m)\right] \qquad r_b < r_{ad}$$

$$G_{jMRo} = \frac{1}{\langle r_b\rangle^m}\left[1-\alpha_q(1-\langle r_b\rangle^m)\right] \qquad r_b > r_{ad}$$

$$G_{jWB} = \frac{2r_e Z}{Nk_L^2 S^2} \qquad Z = 8\pi m_c r_c^2 \quad \text{and} \quad W = \frac{E_0}{B_0^2 R^2}$$

$$\langle r_b\rangle^{(2m+2)} = (ZW)\frac{\left[1-\alpha_q(1-\langle r_b\rangle^m)\right]}{\left[f_0(\langle r_b\rangle)\right]^2} \qquad \langle r_g\rangle^2 = \left[\frac{2WS^2}{r_e\langle r\rangle^{2m}}\right]\frac{\left[1-\alpha_q(1-\langle r\rangle^m)\right]}{\left[f_0(\langle r\rangle)\right]^2}$$

$$\langle r_x\rangle^{(2m+2)} = \left[\frac{NWk_L^2S^2}{2r_e}\right]\frac{\left[1-\alpha_q(1-\langle r_x\rangle^m)\right]}{\left[f_0(\langle r_x\rangle)\right]^2} \qquad S^2 = \overline{\sin^2\varphi}$$

$$\langle r_{ad}\rangle = \langle r_{ad0}\rangle + k_a(\langle r_b\rangle - \langle r_x\rangle) \qquad k_a = \frac{\langle r_k\rangle - \langle r_{ad0}\rangle}{\langle r_k\rangle - \langle r_x\rangle}$$

$$\langle r_{ad0}\rangle^{(2m+2)} = \left[\frac{2m^2}{\Gamma_a^2}\frac{W\beta^2}{r_e}\right]\left[1-\alpha_q(1-\langle r_{ad0}\rangle^m)\right]\left[1+\frac{\langle r_{ad0}\rangle}{m}\frac{f_0'(\langle r_{ad0}\rangle)}{f_0(\langle r_{ad0}\rangle)}\right]$$

$$f_0(\langle r\rangle) = \left[\frac{2}{1+\langle r\rangle^{(m+2)}}\right] \qquad f_0'(\langle r\rangle) = -\frac{2(m+2)\langle r\rangle^{(m+1)}}{\left[1+\langle r\rangle^{(m+2)}\right]^2}$$

Figure 2.

Summary of equations for total electron recirculation ratio, and under mirror reflection (MR) and wiffle–ball (WB) operating modes, and formulae used for critical system radii (gyro, adiabaticity, transition and magnetic pressure balance radii) in "rollover" wells.

Figure 3 a.

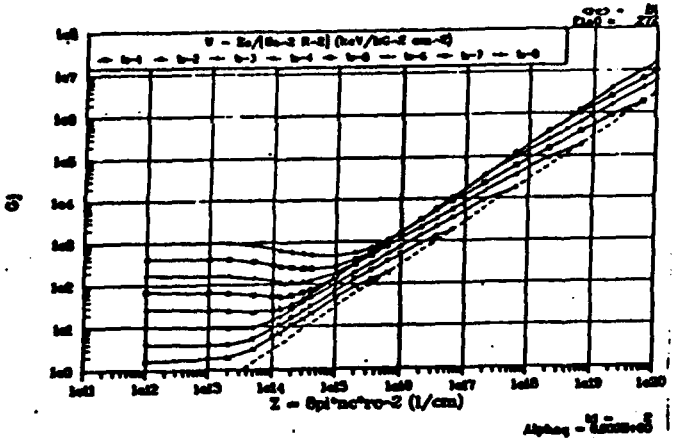

Figure 3 b.

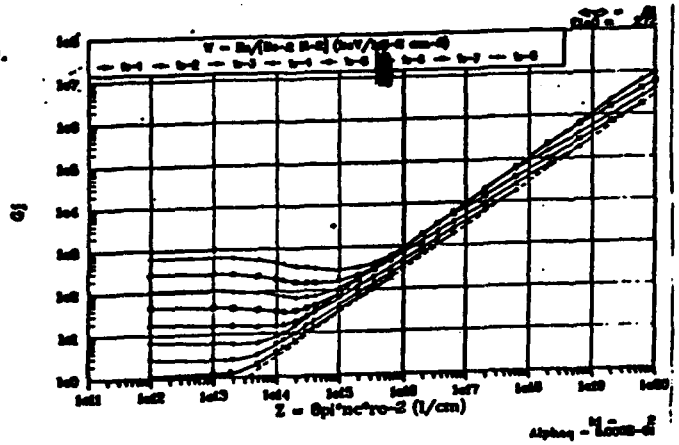

Figure 3 c.

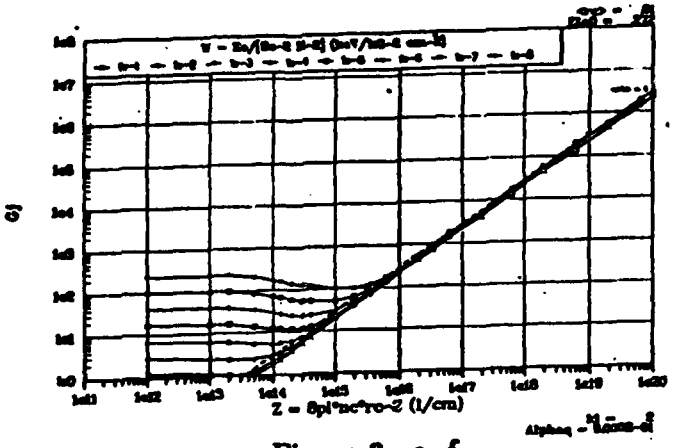

Figure 3 d.

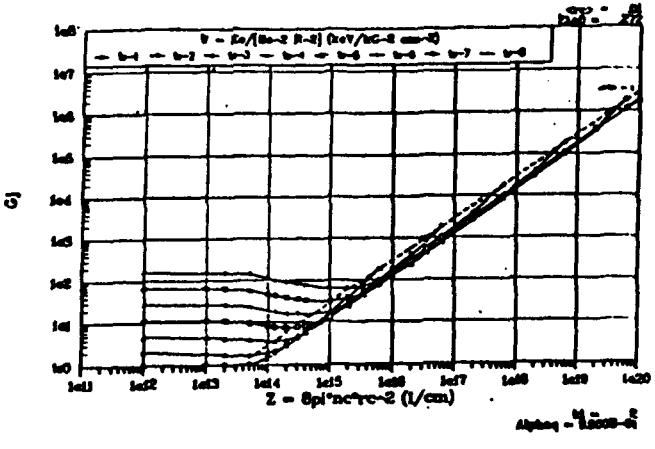

Figure 3 e.

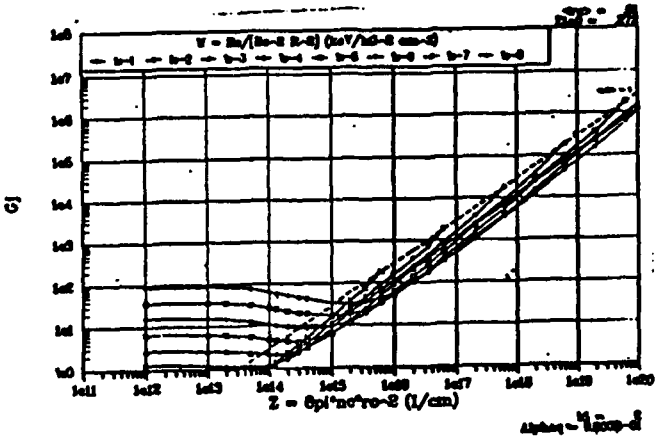

Figure 3 f.

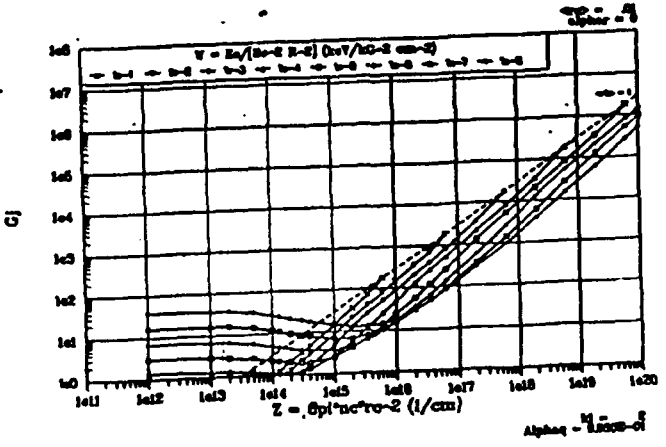

Figure 3. a–f

Effect of well depth, α_q, on G_j vs. Z plots for various values of W. The $\langle r_b \rangle = 1$ line is indicated in each chart by the dashed line.

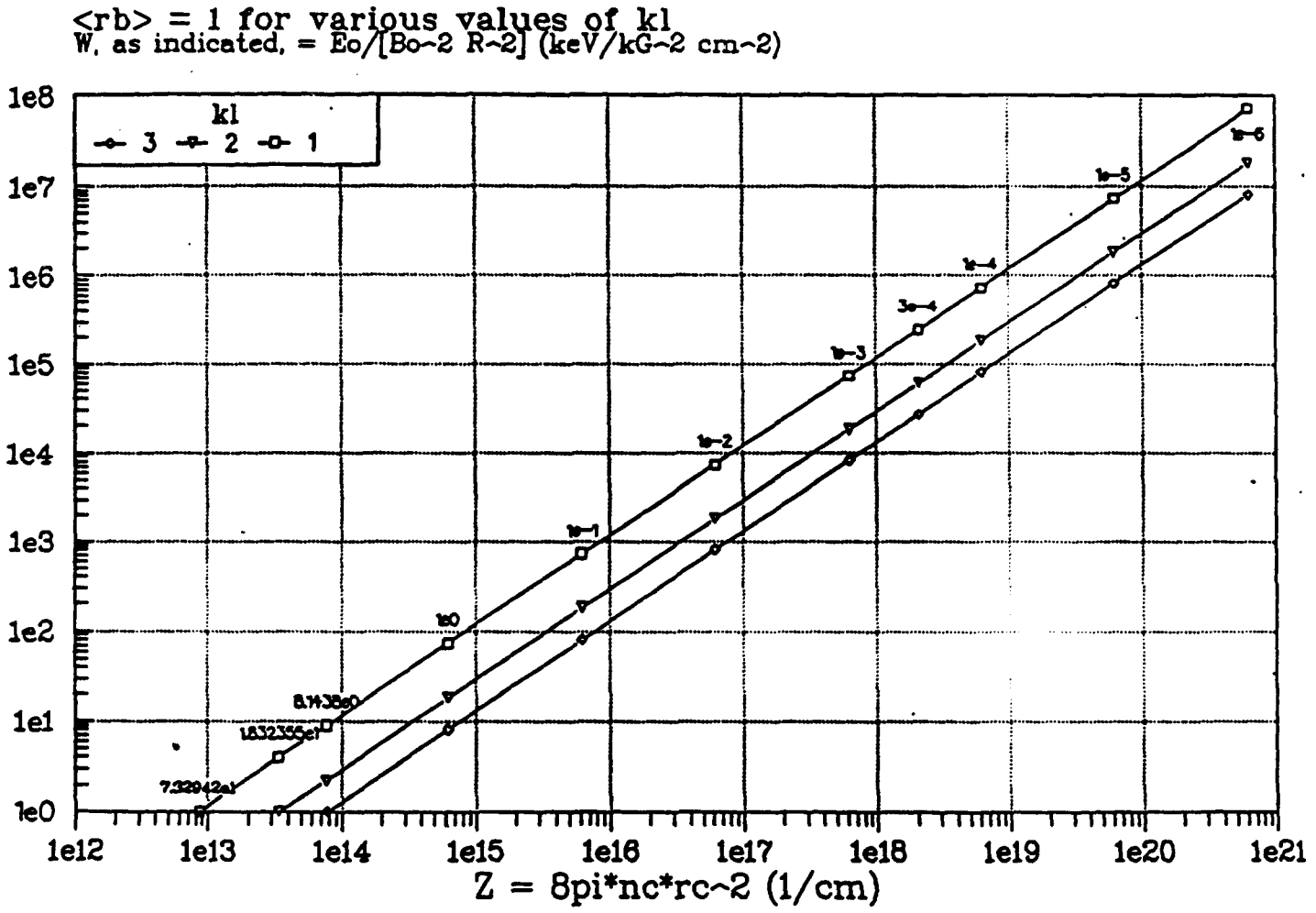

Figure 4.

Effect of gyro "hole" radius, k_L, on G_j vs. Z plots for various values of W. a) The $<r_b> = 1$ line for $k_L = 1, 2, 3$. The magnitude of W at $G_j = 1$ is indicated.

Figure 5.
3–D plot of 2–D projections with k_L=2.

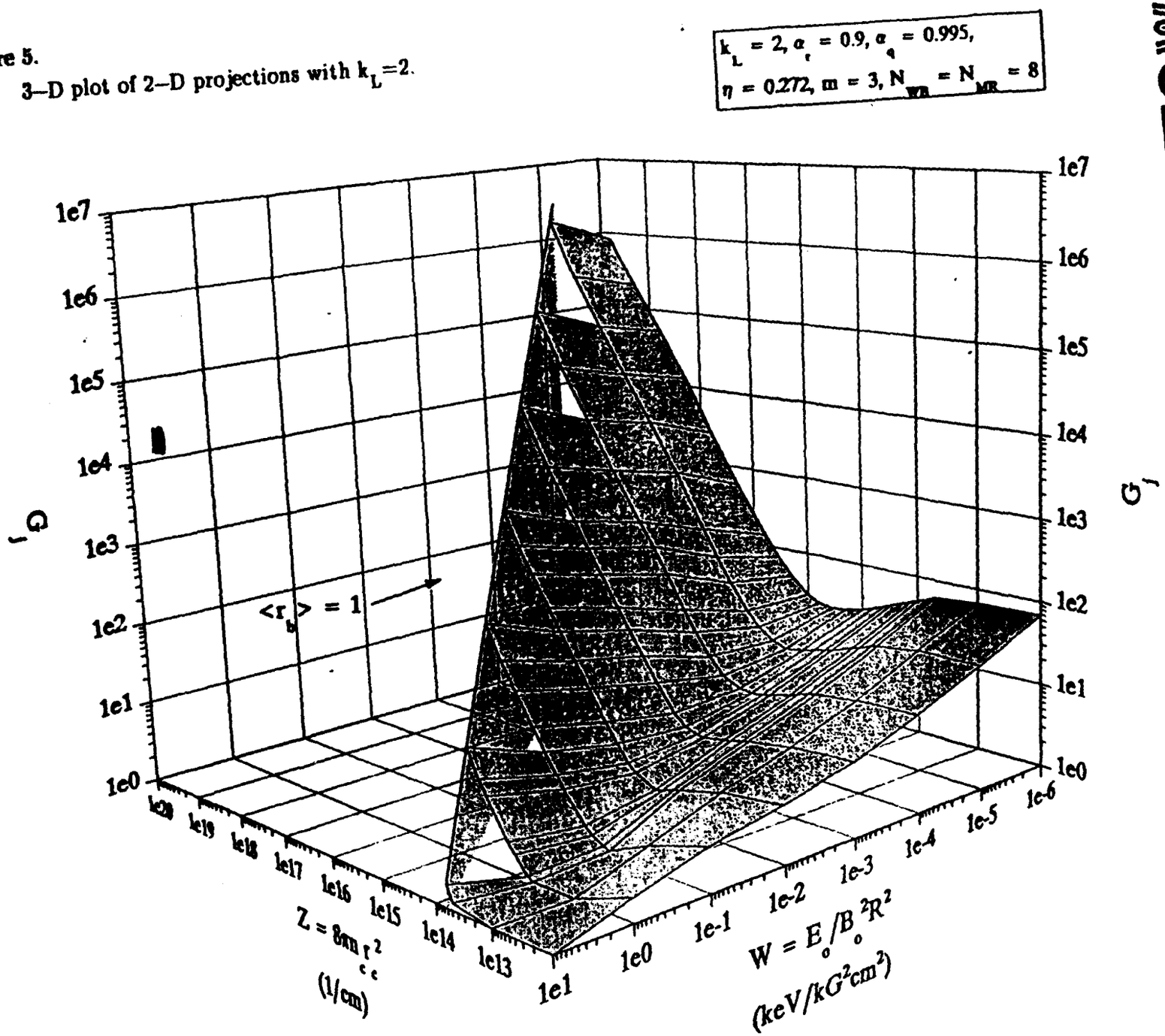

EMC2

Figure 6 a.

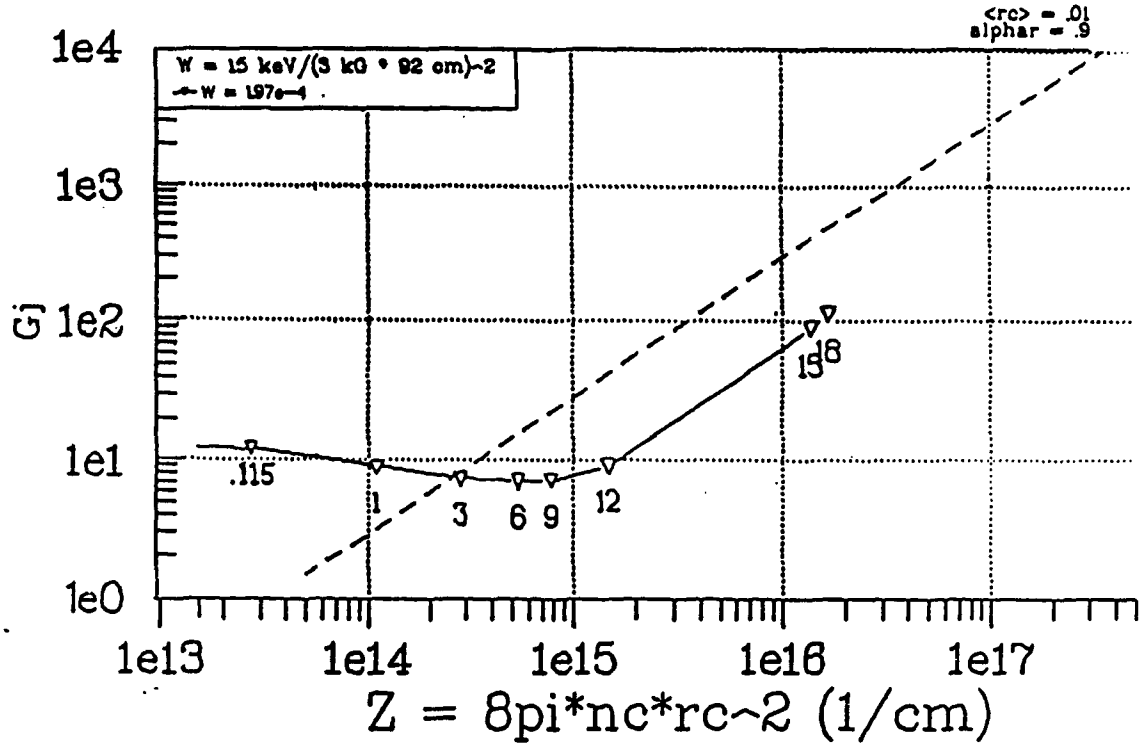

Figure 6 b.

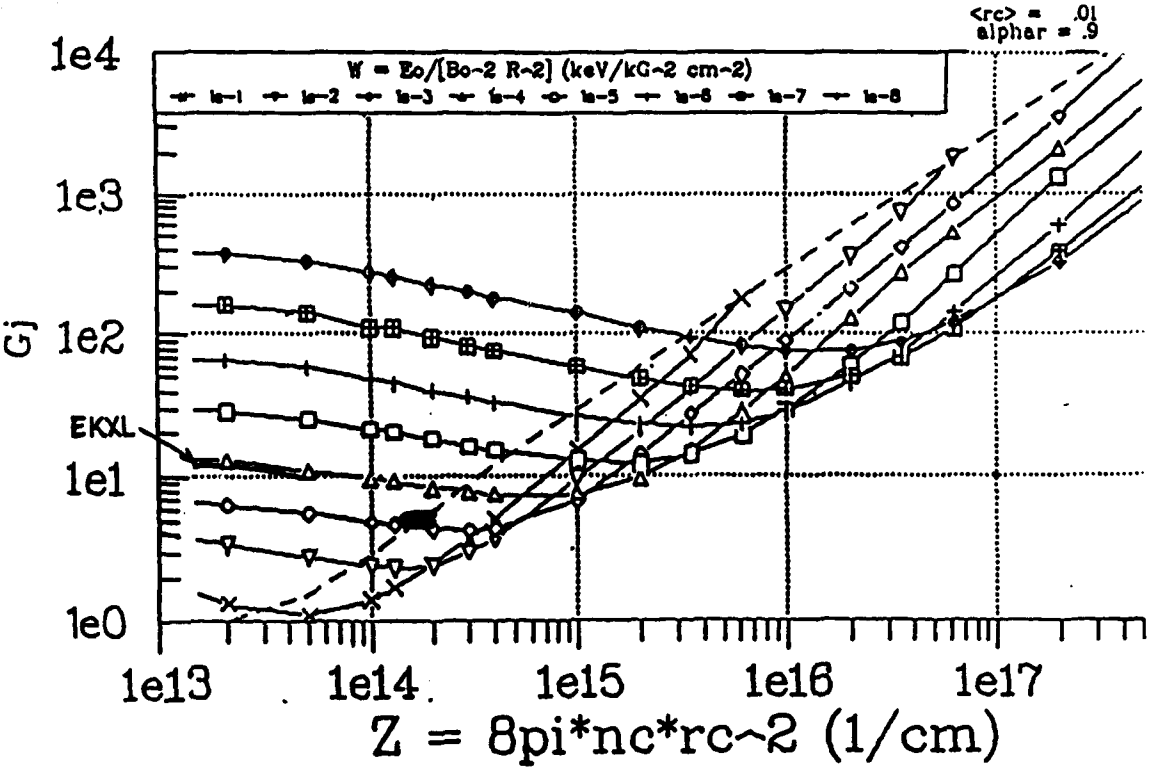

Figure 6. a,b
Increasing drive current necessary to transition from MR to WB mode in a system with a fixed W. Currents given are in kA.